



Chiral discrimination asserted by enantiomers of Ni (II), Cu (II) and Zn (II) Schiff base complexes in DNA binding, antioxidant and antibacterial activities

Noor-ul Hasan Khan^{a,*}, Nirali Pandya^{a,1}, K. Jeya Prathap^{a,1}, Rukhsana Ilays Kureshy^{a,1}, Sayed Hasan Razi Abdi^{a,1}, Sandhya Mishra^{b,1}, Hari Chandra Bajaj^{a,1}

^a Discipline of Inorganic Materials and Catalysis, Central Salt and Marine Chemicals Research Institute (CSMCR), Council of Scientific & Industrial Research (CSIR), G. B. Marg, Bhavnagar-364 021, Gujarat, India

^b Discipline of Marine Biotechnology and Ecology, Central Salt and Marine Chemicals Research Institute (CSMCR), Council of Scientific & Industrial Research (CSIR), G. B. Marg, Bhavnagar-364 021, Gujarat, India

ARTICLE INFO

Article history:

Received 23 February 2011

Received in revised form 13 April 2011

Accepted 2 June 2011

Keywords:

Chiral Schiff base complexes

DNA binding

Superoxide dismutase

Antioxidant activity

Antibacterial activity

ABSTRACT

Chiral Schiff base ligands (*S*)-H₂L and (*R*)-H₂L and their complexes (*S*-Ni-L, *R*-Ni-L, *S*-Cu-L, *R*-Cu-L, *S*-Zn-L and *R*-Zn-L) were synthesized, characterized and examined for their DNA binding, antioxidant and antibacterial activities. The complexes showed higher binding affinity to calf thymus DNA with binding constant ranging from 2.0×10^5 to 4.5×10^6 M⁻¹. All the complexes also exhibited remarkable superoxide (56–99%) and hydroxyl scavenging (45–89%) activities as well as antibacterial activities against gram (+) and gram (–) bacteria. However, none of the complexes showed antifungal activity. Conclusively, *S* enantiomers of the complexes were found to be relatively more efficient for DNA interaction, antioxidant and antibacterial activities than their *R* enantiomers. This study reveals the possible utilization of chiral Schiff base complexes for pharmaceutical applications.

© 2011 Elsevier B.V. All rights reserved.

1. Introduction

One of the life's intrinsic biochemical features is the high selectivity of chiral molecular species. Consequently, many biological responses are greatly influenced by the chirality of the incumbent molecules [1]. It is therefore not surprising to come across incidents where chirality plays a decisive role in the area of pharmaceuticals, agrochemicals, flavors and fragrances. In most of the cases only one optical isomer of the drug molecule selectively interacts with drug-receptor site to show desirable therapeutic activity [2]. Thalidomide—a drug that was prescribed for morning sickness in pregnant women during 1960s is a classic example of this behavior. In this particular case it was found that *R*-enantiomer of thalidomide showed drug action, while *S*-enantiomer caused birth defects [3]. Since then, in medicinal research, all the enantiomers of a chiral compound are considered as different “chemicals” and it has been made mandatory to test each stereoisomer separately for their drug action. Although pharma-sector is dominated by organic molecules as drugs, recently there is a great deal of interest in the biochemical responses of inorganic metal complexes [4]. As a result, bio-manifestation of chiral metal complexes has attracted

the attention of many research groups [5–10]. Studying interaction of chiral metal complexes with biomolecules, particularly with inherently chiral DNA and protein molecules is likely to provide information on chiral discrimination of diastereomers, which may provide important leads for developing targeted bioactive molecules [11–18]. Although, various aspects of chiral discrimination of metal complexes for their binding with DNA and protein molecules have been reported in the past, the role of chirality in free radical scavenging activity and antibacterial activity has not been well explored [12,18]. The deleterious effect of free radicals, particularly superoxide anions (O₂^{•-}) and hydroxyl radical (•OH) in many serious diseases e.g. cerebral- and -cardiovascular disorders, cancer, rheumatoid arthritis and aging etc. [19–21], has encouraged the researcher to study the cooperative effects of chiral metal complexes and to improve their free radical scavenging and antibacterial activities.

While dealing with biological interactions especially in medicinal applications, comparison for the activity of two enantiomers of a complex is crucial. Recently, we have demonstrated influence of chirality on DNA interaction of chiral Ru (II) and Mn (III) salen complexes where one enantiomer of the complex showed better activity than the other enantiomer [12,18]. In view of the above and our ongoing interest in the synthesis of chiral Schiff base metal complexes for various bio-activities, we report here the synthesis of chiral Schiff base ligands (*S*)-H₂L and (*R*)-H₂L and their Ni, Cu and Zn complexes to evaluate their DNA interaction capacity,

* Corresponding author. Tel.: +91 0278 2567760; fax: +91 0278 2566970.

E-mail address: khan251293@yahoo.in (N.-u.H. Khan).

¹ Tel.: +91 0278 2567760; fax: +91 0278 2566970.

antioxidant and antibacterial activities. All the complexes exhibited DNA interaction capacity together with antioxidant and antibacterial activities where was found to be more *S* enantiomer effective. Among all the complexes studied the *S*-Ni-L and *S*-Cu-L metal complexes showed intercalative DNA binding capacity while *R*-Ni-L, *R*-Cu-L, *S*-Zn-L and *R*-Zn-L showed groove or external binding with DNA.

2. Experimental

2.1. Materials and methods

Calf thymus DNA (CT-DNA), (*S*)-(-)- α -methyl benzyl amine and (*R*)-(+)- α -methyl benzyl amine, NBT (nitroblue-tetrazolium) were purchased from Sigma–Aldrich and used as received. EB (ethidium bromide), riboflavin (vitamin B₂), MET (*L*-methionine), trichloro acetic acid, ammonium acetate were purchased from S D Fine Chemicals.

The solution of CT-DNA was prepared in phosphate buffer to give a ratio of UV absorbance at 260 and 280 nm of ca. 1.8–1.9, indicating that the DNA was sufficiently free from protein [18]. DNA concentration per nucleotide was determined by absorption spectroscopy using molar absorption coefficient ($6600 \text{ M}^{-1} \text{ cm}^{-1}$) at 260 nm. All the commercial grade solvents were distilled before use. NMR spectra were done on a Bruker F113V spectrometer (500 MHz, Switzerland) and were referenced internally with TMS. Elemental analysis of complexes was recorded on CHNS Analyzer, PerkinElmer model 2400 (USA). FTIR spectra were recorded on a PerkinElmer Spectrum GX spectrophotometer (USA) in KBr window. High resolution mass spectra were recorded on a LC–MS (USA) (Q–TOF) LC (Waters), MS (Micromass) instruments using acetonitrile as a mobile phase. The spray voltage, tube lens offset, capillary voltage and capillary temperature were set at 4.50 kV, 30.00 V, 23.00 V and 200 °C, respectively, and the *m/z* values were quoted for the major peak in the isotope distribution. UV–vis and fluorescence spectra were recorded on a Shimadzu UV 3101 PC NIR spectrophotometer (Japan) and LS 50B PerkinElmer luminescence spectrophotometer (USA) respectively. Circular dichroism (CD) spectra were measured on a J-815 CD spectrophotometer (Japan) respectively.

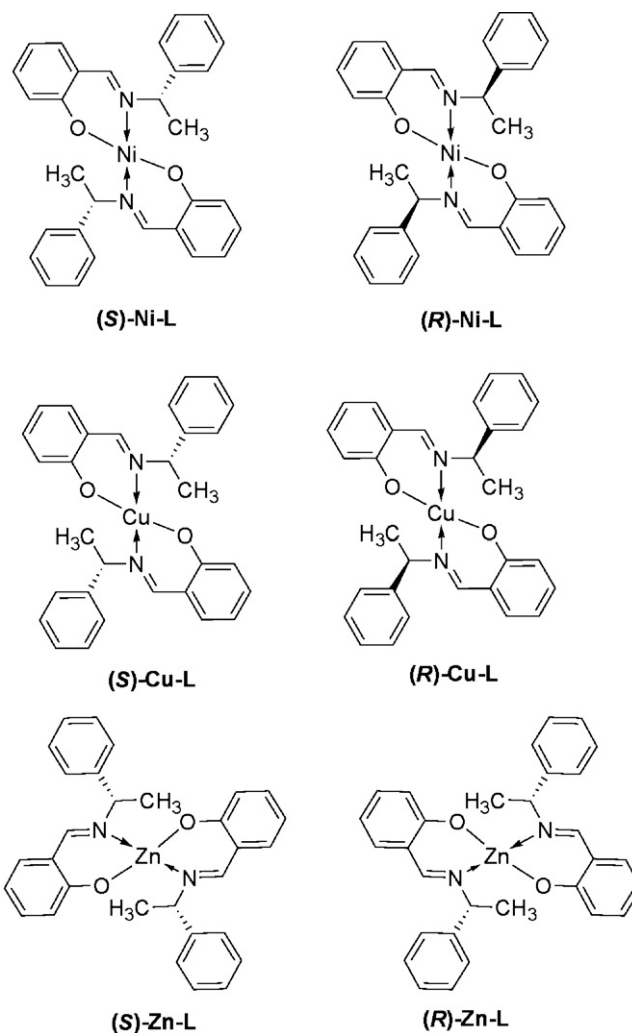
2.2. Synthesis of chiral Schiff base ligands

(*S*)-2-((1-phenylethylimino)methyl)phenol [(*S*)-H₂L] and (*R*)-2-((1-phenylethylimino)methyl)phenol [(*R*)-H₂L]

Ligands (*S*)-H₂L and (*R*)-H₂L were synthesized according to the reported procedure [22]. A solution of salicylaldehyde (16.39 mmol) in absolute ethanol (10 mL) was added to a pre-cooled solution of (*S*)-(-)- α -methyl benzyl amine/(*R*)-(+)- α -methyl benzyl amine (16.39 mmol) in absolute ethanol (10 mL) under vigorous stirring. The resulting solution was subsequently refluxed with stirring for 6–8 h. The completion of the reaction was checked by thin layer chromatography (TLC). After the reaction was completed, the solvent was removed under reduced pressure to get crude ligand, which was washed with hexane (3 × 20 mL) and re-crystallized from methanol to get ligands (*S*)-H₂L and (*R*)-H₂L in sufficiently high purity.

2.3. Synthesis of chiral Schiff base complexes

A solution of nickel acetate (0.665 mmol) in dry methanol (10 mL) was added to the refluxing solution of (*S*)-H₂L/(*R*)-H₂L (1.33 mmol) in dry methanol (5 mL) and the resulting solution was refluxed with stirring for 7–8 h under nitrogen atmosphere. After completion of the reaction (checked on TLC) the solvent was removed under reduced pressure and the residue was re-dissolved



Scheme 1. Structure of chiral Schiff base metal complexes.

in dichloromethane (DCM) and filtered. The filtrate was washed first with distilled water (3 × 5 mL) and finally with brine (saturated sodium chloride) solution. The organic layer was dried over anhydrous sodium sulphate and filtered. Removal of solvent from the filtrate to give a green solid (Scheme 1). Similar method was used to prepare Cu (II) [23] and Zn (II) complexes. The characterization data for the above synthesized complexes are as follows.

2.3.1. (*S*)-H₂L

Yellow solid (89%): IR (KBr $\nu \text{ cm}^{-1}$): 3433, 3033, 2984, 2880, 2365, 1625, 1572, 1491, 1454, 1375, 1276, 1203, 1078, 970, 848, 761, 644, 535; ¹H NMR (500 MHz, CDCl₃, δ ppm): 13.57 (s, 1H, OH), 8.406 (s, 1H, H–C=N), 7.36–6.86 (m, 9H, aromatic), 4.60–4.56 (q, *J* = 6.8 Hz, 1H, CH), 4.54–4.50 (q, *J* = 6.6 Hz, 1H, CH), 1.65–1.61 (d, *J* = 6.6 Hz, 3H, CH₃); Analysis. Calcd for C₁₅H₁₅NO: C, 79.97; H, 6.71; N, 6.22. Found: C, 80.02; H, 6.65; N, 6.18; MS (ESI) *m/z* = 225 [M]⁺; UV–vis λ_{max} : 255 (14,192), 325 (3752) nm.

2.3.2. (*R*)-H₂L

Yellow solid (90%): IR (KBr $\nu \text{ cm}^{-1}$): 3432, 3034, 2985, 2880, 2367, 1624, 1573, 1493, 1451, 1376, 1278, 1080, 971, 845, 760, 645, 537; ¹H NMR (500 MHz, CDCl₃, δ ppm): 13.56 (s, 1H, OH), 8.41 (s, 1H, H–C=N), 7.32–6.83 (m, 9H, aromatic), 4.60–4.56 (q, *J* = 6.8 Hz, 1H, CH), 4.53–4.50 (q, *J* = 6.6 Hz, 1H, CH), 1.64–1.61 (d, *J* = 6.6 Hz, 3H, CH₃); Analysis. Calcd for C₁₅H₁₅NO: C, 79.97; H, 6.71; N, 6.22.

Found: C, 79.95; H, 6.68; N, 6.18; MS (ESI) $m/z = 225 [M]^+$; UV-vis λ_{\max} : 255 (13,330), 325 (3406) nm.

2.3.3. (S)-Ni-L

Green solid (80%): IR (KBr ν cm^{-1}): 3393, 2977, 2934, 1573, 1413, 1280, 1198, 1153, 1028, 937, 889, 809, 758, 679, 617; ^1H NMR (500 MHz, CDCl_3 , δ ppm): 8.416 (s, 1H, H-C=N), 7.37–6.83 (m, 18H, aromatic), 4.61–4.57 (q, $J = 6.6$ Hz, 1H, CH), 4.54–4.51 (q, $J = 6.6$ Hz, 1H, CH), 1.65–1.62 (d, $J = 6.6$ Hz, 3H, CH_3); ^{13}C NMR (500 MHz, CDCl_3) δ 164.11, 161.81, 144.52, 132.96, 132.05, 129.36, 127.94, 127.09, 119.28, 117.68, 69.19, 25.59; Analysis. Calcd for $\text{C}_{30}\text{H}_{28}\text{N}_2\text{O}_2\text{Ni}$: C, 71.03; H, 5.56; N, 5.52. Found: C, 71.01; H, 5.52; N, 5.48; MS (ESI) $m/z = 507 [M]^+$; UV-vis λ_{\max} : 276 (19,440), 324 (3638), 393 (9046) nm.

2.3.4. (R)-Ni-L

Green solid (78%): IR (KBr ν cm^{-1}): 3391, 2975, 2933, 1575, 1413, 1338, 1197, 1153, 1081, 1028, 936, 890, 857, 758, 678, 616, 526; ^1H NMR (500 MHz, CDCl_3 , δ ppm): 8.42 (s, 1H, H-C=N), 7.38–6.84 (m, 18H, Aromatic), 4.61–4.58 (q, $J = 6.6$ Hz, 1H, CH), 4.55–4.51 (q, $J = 6.6$ Hz, 1H, CH), 1.66–1.62 (d, $J = 6.6$ Hz, 3H, CH_3); ^{13}C NMR (500 MHz, CDCl_3) δ 164.13, 161.82, 144.54, 132.99, 132.08, 129.37, 127.98, 127.11, 119.30, 117.69, 69.20, 25.61; Analysis Calcd for $\text{C}_{30}\text{H}_{28}\text{N}_2\text{O}_2\text{Ni}$: C, 71.03; H, 5.56; N, 5.52. Found: C, 70.91; H, 5.52; N, 5.48; MS (ESI) $m/z = 507 [M]^+$; UV-vis λ_{\max} : 276 (18,126), 324 (3692), 393 (7952) nm.

2.3.5. (S)-Cu-L

Dark Green solid (79%): IR (KBr ν cm^{-1}): 3437, 2969, 2927, 1618, 1534, 1449, 1398, 1326, 1197, 1097, 1025, 888, 751, 697, 592; Analysis. Calcd for $\text{C}_{30}\text{H}_{28}\text{N}_2\text{O}_2\text{Cu}$: C, 70.36; H, 5.51; N, 5.51. Found: C, 70.34; H, 5.49; N, 5.47; MS (ESI) $m/z = 512 [M]^+$; UV-vis λ_{\max} : 277 (36,830), 315 (21,710), 386 (20,240) nm.

2.3.6. (R)-Cu-L

Dark Green solid (75%): IR (KBr ν cm^{-1}): 3433, 2968, 2930, 1615, 1532, 1451, 1326, 1326, 1197, 1077, 1026, 928, 890, 750, 697, 595; Analysis. Calcd for $\text{C}_{30}\text{H}_{28}\text{N}_2\text{O}_2\text{Cu}$: C, 70.36; H, 5.51; N, 5.51. Found: C, 70.31; H, 5.49; N, 5.49; MS (ESI) $m/z = 512 [M]^+$; UV-vis λ_{\max} : 279 (30,128), 315 (21,560), 386 (20,460) nm.

2.3.7. (S)-Zn-L

Dark Yellow solid (76%): IR (KBr ν cm^{-1}): 3633, 3433, 3033, 2880, 2358, 1622, 1578, 1493, 1453, 1378, 1277, 1079, 970, 912, 760, 697, 536, 447; ^1H NMR (500 MHz, CDCl_3 , δ ppm): 8.42 (s, ^1H , H-C=N), 7.38–6.83 (m, 18H, Aromatic), 4.61–4.58 (q, $J = 6.6$ Hz, 1H, CH), 4.54–4.51 (q, $J = 6.6$ Hz, 1H, CH), 1.66–1.62 (d, $J = 6.6$ Hz, 3H, CH_3); ^{13}C NMR (500 MHz, CDCl_3) δ 164.19, 144.58, 133.03, 129.42, 128.01, 127.14, 119.36, 117.72, 69.24, 25.69; Analysis. Calcd for $\text{C}_{30}\text{H}_{28}\text{N}_2\text{O}_2\text{Zn}$: C, 70.11; H, 5.49; N, 5.45. Found: C, 70.08; H, 5.44; N, 5.39; MS (ESI) $m/z = 514 [M]^+$; UV-vis λ_{\max} : 276 (22,568), 322 (5066), 392 (11,506) nm.

2.3.8. (R)-Zn-L

Dark Yellow (78%): IR (KBr ν cm^{-1}): 3631, 3429, 3033, 2879, 2360, 1621, 1492, 1451, 1378, 1276, 1079, 971, 913, 760, 694, 535, 444; ^1H NMR (500 MHz, CDCl_3 , δ ppm): 8.42 (s, 1H, H-C=N), 7.38–6.84 (m, 18H, Aromatic), 4.62–4.58 (q, $J = 6.6$ Hz, 1H, CH), 4.55–4.52 (q, $J = 6.6$ Hz, 1H, CH), 1.66–1.63 (d, $J = 6.6$ Hz, 3H, CH_3); ^{13}C NMR (500 MHz, CDCl_3) δ 164.21, 144.59, 133.05, 129.44, 128.04, 127.16, 119.39, 117.73, 69.27, 25.70; Analysis. Calcd for $\text{C}_{30}\text{H}_{28}\text{N}_2\text{O}_2\text{Zn}$: C, 70.11; H, 5.49; N, 5.45. Found: C, 70.02; H, 5.42; N, 5.41; MS (ESI) $m/z = 514 [M]^+$; UV-vis λ_{\max} : 276 (22,736), 322 (5104), 392 (10,370) nm.

2.4. DNA binding experiments

The stock solution of chiral Schiff base complexes in DMSO (10 mmol) were used for spectroscopic titration of DNA solution in phosphate buffer (10 mM, pH 7.0), by keeping the concentration of DMSO as 0.5% throughout the experiments. Accordingly, incremental quantity of DNA solution 0–55 μM was added to the fixed concentration of chiral Schiff base metal complex solution S-Ni-L/R-Ni-L/S-Cu-L/R-Cu-L/S-Zn-L/R-Zn-L (50 μM) and the spectra were recorded at 250–500 nm. The intrinsic binding constant was determined by monitoring the changes of absorbance at LMCT position.

DNA quenching experiments in the presence of EB was carried out in phosphate buffer (10 mM, pH 7.0) by keeping the fixed concentration of EB solution (4 μM), DNA (100 μM) but varying the concentration of chiral Schiff base metal complexes (S-Ni-L and R-Ni-L (0–25 μM) and S-Cu-L, R-Cu-L, S-Zn-L and R-Zn-L (0–220 μM)) respectively. The emission spectra were recorded at 500–700 nm where the excitation wavelength was kept at 478 nm.

Circular dichroism (CD) spectra were recorded on a Jasco J-815 spectrometer at a scanning speed of 50 nm/min at room temperature using fixed concentration of the chiral Schiff base complexes (50 μM) in DMSO in the absence and presence of increasing amount of DNA (0–60 μM). Each CD spectrum has been subtracted with that of free DNA and thus the spectrum purely reflect the changes in the enantiomer of the complex upon binding with DNA.

Viscosity measurements were conducted on Ostwald's viscometer at 30 ± 0.01 °C using fixed concentration of DNA solution (50 μM) with increasing concentration of chiral Schiff base metal complexes S-Ni-L/R-Ni-L/S-Cu-L/R-Cu-L/S-Zn-L/R-Zn-L (0–60 μM) in phosphate buffer (10 mM, pH 7.0) for flow time measurements. Each sample was measured in triplicate and the average flow time was calculated with a digital stopwatch. Data were presented as $(\eta/\eta_0)^{1/3}$ versus the ratio of the concentration of the compound and DNA, where η is the viscosity of DNA in the presence of the complex, and η_0 is the viscosity of DNA alone [24].

To determine the stability of DNA, thermal denaturation experiments were carried out on a TCC 260 temperature controller programmer on UV-3101 PC spectrophotometer by mixing the solutions of metal complex S-Ni-L/R-Ni-L/S-Cu-L/R-Cu-L/S-Zn-L/R-Zn-L (20 μM) and solution of DNA (0.4 mM) in phosphate buffer (10 mM, pH 7.0). The resulting mixture was incubated for 2 min at different temperatures (35–95 °C) and the absorption intensity was recorded at 260 nm. The T_m value was determined from the graph at the midpoint of temperature curve.

2.5. Antioxidant activity

2.5.1. Scavenger measurements of superoxide radical and hydroxyl radical

The superoxide radicals were generated in the test system using NBT/VitB₂/MET and determined spectrometrically by nitroblue tetrazolium photo reduction method [18,21,25]. The suppression of superoxide radicals was calculated by measuring the absorbance at 560 nm. The chiral metal complexes S-Ni-L/R-Ni-L/S-Cu-L/R-Cu-L/S-Zn-L/R-Zn-L (5–25 μM) were added to a solution containing [NBT (65 μM), L-MET (13 mM), VitB₂ (1.5 μM), EDTA (0.1 mM)] and the resulting solution was made up to 2 mL with phosphate buffer (10 mM, pH 7.0) in dark. The above mixture was illuminated with a white fluorescence lamp (15 W) for 15 min and the absorbance (A_i) was measured at 560 nm. The above mixture containing no metal complex was used as a control and its absorbance was taken as A_0 . All the experiments were conducted in triplicate and data were

expressed as mean and standard deviation. The suppression ratio was calculated by using following equation.

$$\text{O}_2^{\bullet-} \text{ scavenging activity (\%)} = \left[\frac{A_0 - A_i}{A_0} \times 100 \right] \quad (1)$$

The hydroxyl radical scavenging study was carried out by reported procedure [26] with minor modification. The formaldehyde formed during the oxidation of dimethyl sulphoxide by the Fe^{3+} -ascorbic acid was used to measure the concentration of generated hydroxyl radical [27]. A solution of 0.1 mM EDTA/167 mM Fe^{3+} (as a 1:2 mixture with EDTA)/33 mM DMSO in phosphate buffer (150 mM, pH 7.4) was mixed with the varying concentration of the chiral Schiff base metal complexes and the reaction was initiated by the addition of 2 mM ascorbic acid. The resulting mixture was incubated for 30 min at 37 °C. After completion of the reaction, 125 μL trichloroacetic acid (17.5%, w/v) was added to quench the reaction. The formaldehyde thus formed was assayed spectrophotometrically by the method of Nash [28]. All the experiments were performed in triplicate with appropriate controls and the following expression was used to calculate hydroxyl radical scavenging activity.

$$\bullet\text{OH scavenging activity (\%)} = \left[\frac{A_0 - A_i}{A_0} \times 100 \right] \quad (2)$$

2.6. Antibacterial activity

The agar cup method was employed to determine the antimicrobial activities of Schiff base metal complexes against the three gram (+), three gram (–) and two fungal organisms. Broth micro dilution method was used to determine the MICs (minimum inhibitory concentrations) for the complexes dissolved in DMSO against test organisms. All the tests were performed in duplicate and modal values were selected. Each microorganism was inoculated on to the surface of Nutrient agar (N-agar). The wells (6 mm in diameter) were cut from the agar and 0.1 mL solution of complex was delivered in to them. After incubation for 24 h (48 h for fungi) at 37 °C, all the plates were examined for the zone of growth inhibition, and diameters of these zones were measured in millimeter.

3. Results and discussion

3.1. Synthesis and general properties

The chiral Schiff base metal complexes S-Ni-L, R-Ni-L, S-Cu-L, R-Cu-L, S-Zn-L and R-Zn-L were prepared in high yields (~70%) by the reaction of the chiral Schiff base ligands (S)-(H₂L)/(R)-(H₂L) with Ni (II), Cu (II) and Zn (II) acetates respectively (Scheme 1). The complexes were characterized by various spectroscopic and analytical techniques (data is given in experimental section). All the complexes displayed the molecular ion peak corresponding to $[\text{M}]^+$ in their ESI-MS spectra. IR spectra of the ligands showed two characteristic peak near 1626 and 3300 cm^{-1} assigned to ν (H-C=N) and ν (OH) respectively. After coordination with metal ions, the characteristic ν (H-C=N) peak shifted to lower wave number while the intensity of phenolic OH peak diminished significantly, confirming its involvement in complex formation. The ¹H NMR spectrum of the chiral Schiff base ligand, showed singlet at δ 13.57 for its OH proton and azomethine proton was appeared as a singlet at δ 8.41 ppm. The CH proton was appeared as quartet at δ 4.60 (q, J = 6.8 Hz) and 4.54 (J = 6.6 Hz) and CH₃ protons were appeared as doublet at δ 1.65 (J = 6.6 Hz). After coordination with metal ions, the characteristic ν (H-C=N) peak in IR was shifted to lower wave number and phenolic OH peak decreased significantly confirming the coordination through azomethine nitrogen and phenolic oxygen atoms. The UV-vis spectra of chiral Schiff base ligands and chiral complexes

S-Ni-L, R-Ni-L, S-Cu-L, R-Cu-L, S-Zn-L and R-Zn-L were recorded in aqueous DMSO (0.5%). The chiral Schiff base ligands showed characteristic charge transfer (CT) bands at 255 nm and 326 nm, however, in the complex formation the peaks were shifted to 275–277 nm and 315–325 nm respectively. After coordination with metal ions generate new broad ligand to metal charge transfer (LMCT) peak at the position of 380–400 nm.

3.2. Solubility and stability

The complexes were highly soluble in MeOH, EtOH, DMF, DMSO, CH₂Cl₂ and DCM. The aqueous DMSO solution of these complexes did not show any change in their UV-vis spectrum profile over a period of 48 h at ambient temperature demonstrating the stability of these complexes under ambient condition (data is given in Supporting Information as Figs. S1–S3).

3.3. DNA binding and antioxidant activity

3.3.1. Electronic absorption spectroscopy

The change in absorbance and shift in wavelength after the addition of increasing concentration of DNA solution in a fixed concentration of chiral metal complexes gave valuable information on the mode of interaction [29]. Strong intercalative binding of small molecule to DNA is known to cause much larger shifts and hypochromism of the spectral bands [29–31]. The absorption spectra of chiral Schiff base metal complexes S-Ni-L, R-Ni-L, S-Cu-L, R-Cu-L, S-Zn-L and R-Zn-L with increasing concentration of DNA showed hypochromism at LMCT position (Figs. 1–3). Interestingly, hypochromism at LMCT position of complex S-Ni-L was associated with a major blue shift, while complex S-Cu-L displayed major red shift suggesting their intercalative mode of binding (Table 1). However, complexes R-Ni-L, R-Cu-L, S-Zn-L and R-Zn-L showed minor hypochromism and minor shift at LMCT band, indicating mainly groove binding or non-intercalative nature of these complexes. Interestingly, in the presence of DNA, complexes S-Ni-L and R-Ni-L showed hyperchromism at 324 nm while S-Zn-L and R-Zn-L showed hyperchromism at 322 nm. The complexes S-Cu-L and R-Cu-L showed hypochromism at the position of 315 nm. Among all the complexes used in the present study the S-Ni-L complex showed strongest interaction with DNA.

The absorbance at LMCT position of the complexes was used to calculate the intrinsic binding constant using following functional equation [32].

$$\frac{[\text{DNA}]}{(\varepsilon_a - \varepsilon_f)} = \frac{[\text{DNA}]}{(\varepsilon_b - \varepsilon_f)} + \frac{1}{K_b(\varepsilon_b - \varepsilon_f)} \quad (3)$$

where [DNA] is the concentration of DNA in base pairs, ε_a , ε_f and ε_b correspond to $A_{\text{obs}}/[\text{M}]$, the extinction coefficient of the free chiral Schiff base metal complex, and the extinction coefficient of the chiral Schiff base metal complex in the fully bound form, respectively. The K_b was obtained from the ratio of slope to intercept by using the plot of $[\text{DNA}]/(\varepsilon_a - \varepsilon_f)$ versus [DNA]. The binding constant (K_b) of the chiral Schiff base metal complexes with DNA are given in Table 1. The K_b values of the complexes S-Ni-L and S-Cu-L were found to be in the range of classical intercalator ethidium bromide (EB, $K_b = 1.4 \times 10^6 \text{ M}^{-1}$) [32] suggesting their intercalative binding while the lower K_b values showed by rest of the complexes (R-Ni-L, R-Cu-L, S-Zn-L, R-Zn-L) evident their groove or external binding nature. Among all the complexes studied, the S-enantiomers had better binding efficiency than their R counter parts.

3.3.2. Determination of thermodynamic parameters

The thermodynamic parameters were further used to understand the nature of binding forces between the chiral Schiff base metal complexes with DNA. Standard entropy changes (ΔS°) and

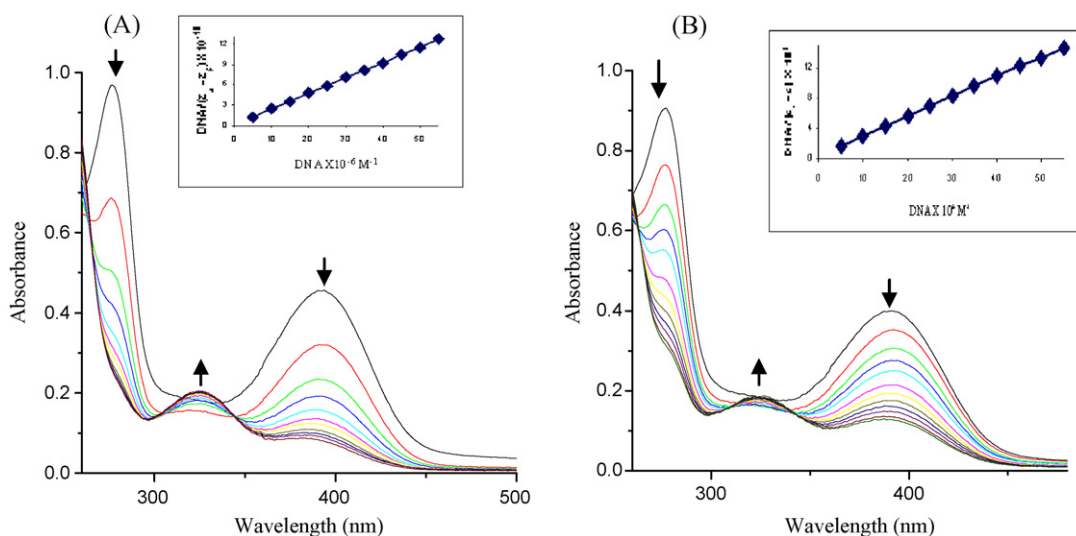


Fig. 1. Absorption spectra of chiral Ni (II) Schiff base complexes (50 μM) (A) *S*-Ni-L (B) *R*-Ni-L in phosphate buffer (10 mM, pH 7.0) in the presence of increasing concentration of DNA (0–55 μM). Inset plot is $[\text{DNA}]/(\epsilon_a - \epsilon_f)$ vs. DNA.

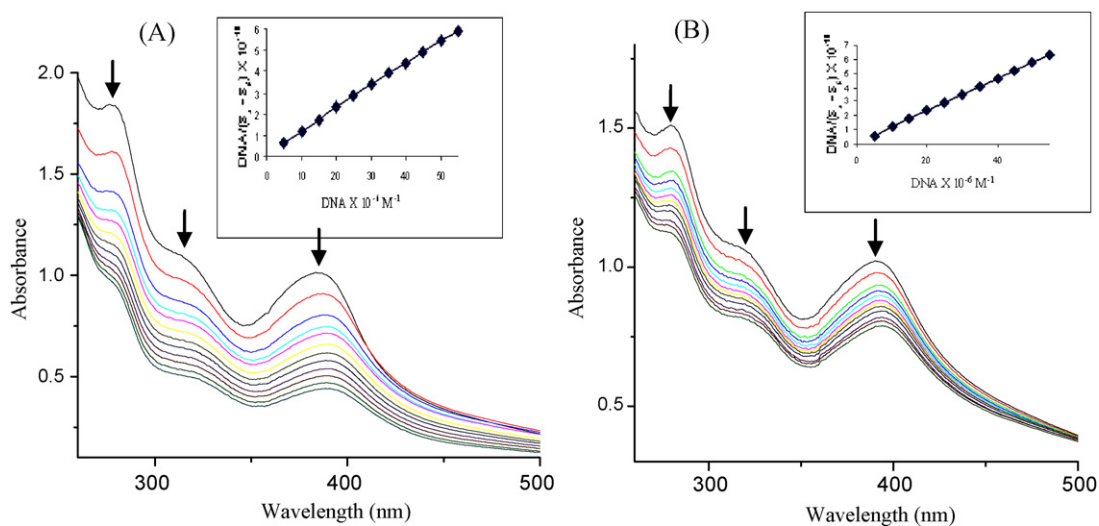


Fig. 2. Absorption spectra of chiral Cu (II) Schiff base complexes (50 μM) (A) *S*-Cu-L (B) *R*-Cu-L in phosphate buffer (10 mM, pH 7.0) in the presence of increasing concentration of DNA (0–55 μM). Inset plot is $[\text{DNA}]/(\epsilon_a - \epsilon_f)$ vs. DNA.

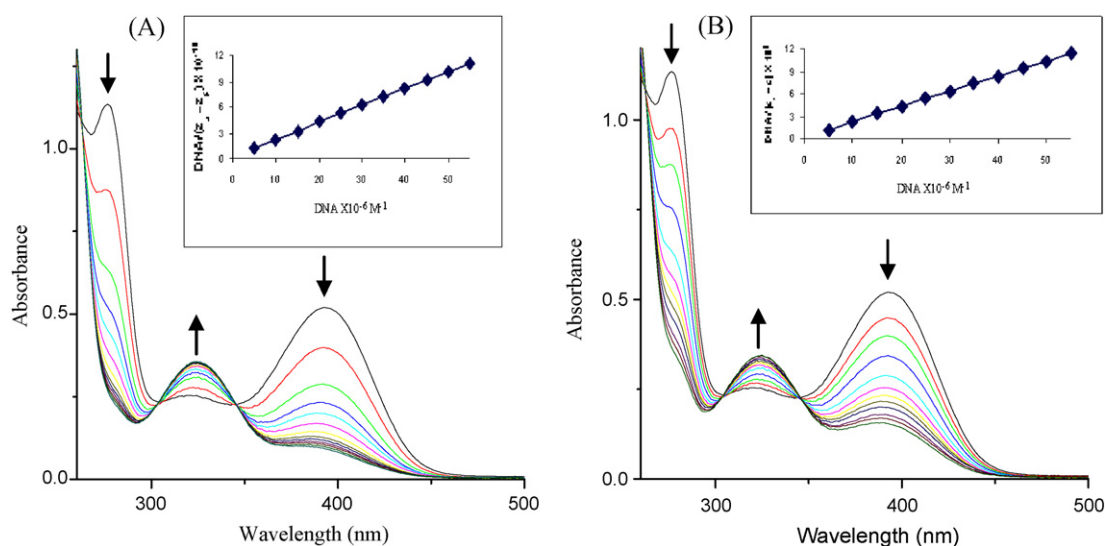


Fig. 3. Absorption spectra of chiral Zn (II) Schiff base complexes (50 μM) (A) *S*-Zn-L (B) *R*-Zn-L in phosphate buffer (10 mM, pH 7.0) in the presence of increasing concentration of DNA (0–55 μM). Inset plot is $[\text{DNA}]/(\epsilon_a - \epsilon_f)$ vs. DNA.

Table 1
Binding constant of S and R enantiomers of chiral Schiff base metal complexes.

Entry	Complexes	λ_{\max}	λ_{\max} (DNA + complexes)	$\Delta\lambda$ (nm)	$K_b \times M^{-1}$
1	S-Ni-L	276, 324, 393	277, 326, 385	1, 2, 8	$4.5 (\pm 0.9) \times 10^6$
2	R-Ni-L	276, 324, 393	276, 324, 390	0, 0, 3	$5.1 (\pm 0.9) \times 10^5$
3	S-Cu-L	277, 315, 386	278, 316, 392	1, 1, 6	$1.06 (\pm 0.4) \times 10^6$
4	R-Cu-L	277, 315, 386	277, 315, 389	0, 0, 3	$2.3 (\pm 0.5) \times 10^5$
5	S-Zn-L	276, 322, 392	276, 324, 389	0, 2, 4	$6.5 (\pm 0.8) \times 10^5$
6	R-Zn-L	276, 322, 392	276, 322, 389	0, 0, 3	$2.0 (\pm 0.5) \times 10^5$

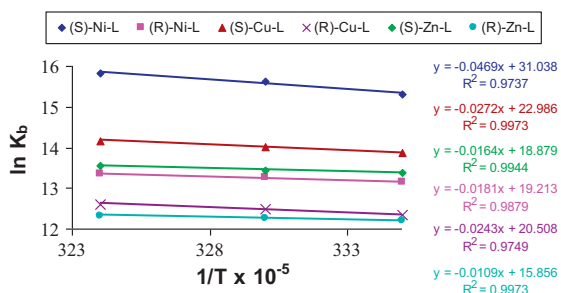


Fig. 4. The Van't Hoff plot for the interaction of chiral Schiff base metal complexes with DNA.

standard enthalpy changes (ΔH°) between complex and DNA are interpreted in three ways: (i) ΔH and $\Delta S > 0$ (endothermic) indicates that the interaction is originated from hydrophobic forces, (ii) ΔH and $\Delta S < 0$ (exothermic) is interpreted in term of van der Waals interactions and hydrogen bond being major source of DNA interaction, and (iii) if $\Delta H < 0$ and $\Delta S > 0$, the electrostatic forces are dominant factor for the interaction between complex with DNA [33]. The temperature dependent binding constant was measured and following relation was used to calculate Gibbs free energy.

$$\Delta G^\circ = -RT \ln K_b \quad (4)$$

In the above equation R , T and K_b are the gas constant, temperature and binding constant respectively. The binding enthalpy of chiral Schiff base metal complexes was calculated by using slope of the Van't Hoff equation and binding entropy was calculated from the intercept of linear Van't Hoff equation as given below. The graph is given in Fig. 4. The detail calculations for DNA binding with (S)-

Ni-L and (R)-Ni-L are given in supporting information in Section 1. Similar calculations were followed for other complexes as well.

$$\ln K_b = -\frac{\Delta H^\circ}{RT} + \frac{\Delta S^\circ}{R} \quad (5)$$

The data in Table 2, S1 and S2 showed negative value of ΔG° and positive value of ΔS° and ΔH° for S-Ni-L, R-Ni-L, S-Cu-L, R-Cu-L, S-Zn-L, and R-Zn-L complexes indicated that the reaction process is spontaneous and the binding is mainly entropy driven. Therefore, it is inferred that the hydrophobic interaction plays a major role in the binding of Schiff base complexes with DNA [34].

3.3.3. Fluorescence quenching studies

The EB displacement assay usually used to determine Stern–Volmer constant of the complexes to bind with DNA particularly when the complexes failed to show any luminescence upon excitation of CT and LMCT band. In the present study, the solutions of chiral Schiff base complexes S-Ni-L, R-Ni-L, S-Cu-L, R-Cu-L, S-Zn-L and R-Zn-L in different solvents did not show any luminescence irrespective of the presence and absence of DNA. Therefore, EB which is known to emit intense fluorescence in the presence of DNA due to the strong intercalation of EB between the base pairs of DNA was used as a spectral probe [30]. The intense fluorescence obtained by the interaction of EB and DNA got diminished by the addition of chiral Schiff base complexes (Fig. 5) suggesting their competitive binding [35]. Also the addition of increasing concentration of the chiral Schiff base metal complexes to EB solution in the absence of DNA result in no change in the emission intensity of EB, thus evident for no interaction between the metal complex and EB. The complexes S-Ni-L and R-Ni-L were found to have stronger binding capacity at 0–25 μM concentration than other complexes which required relatively higher concentrations (0–220 μM , Figs. S4 and S5) to get comparable decrease in emission intensity.

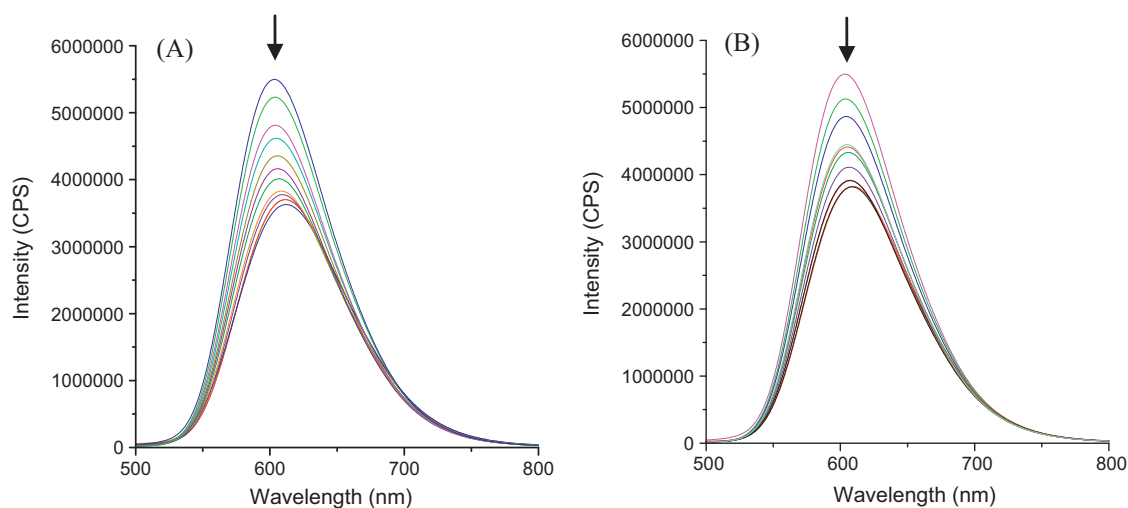


Fig. 5. The emission spectra of DNA bound EB in the presence of (A) S-Ni-L (B) R-Ni-L in phosphate buffer (10 mM, pH 7.0) in the presence of increasing concentration of complexes (0–25 μM). DNA = 100 μM .

Table 2
Thermodynamic parameters and binding constant of chiral Schiff base complexes S-Ni-L and^a R-Ni-L to DNA in phosphate buffer (10 mM, pH 7.0).

T (K)	K_b	ΔG° (kJ mol ⁻¹)	ΔH° (kJ mol ⁻¹)	ΔS° (J mol K ⁻¹)
298	4.5×10^6 (5.18×10^5)M ⁻¹	-37.95 (-32.60)	38.99 (15.04)	257.99 (159.74)
303	6.1×10^6 (5.78×10^5)M ⁻¹	-39.36 (-33.42)		
308	7.5×10^6 (6.3×10^5)M ⁻¹	-40.539 (-34.19)		

^a Results in parenthesis are for R-Ni-L enantiomer.

Based on Figs. 5, S4 and S5 the Stern–Volmer constant were calculated by using following functional equation [3].

$$\frac{I_0}{I} = 1 + K \cdot r \quad (6)$$

In the above equation I_0 and I are the emission intensities in the absence and presence of chiral Schiff base metal complexes and r is the ratio of the total concentration of chiral metal complexes to DNA and K is given by the ratio of slope to the intercept (data is given in Table 3).

The Stern–Volmer constant value for S-Ni-L was higher than rest of the complexes. Moreover, S-enantiomers showed stronger binding with DNA than their R-counterparts in all the complexes, suggesting that the DNA which is essentially chiral in nature indeed show stereochemical preference for binding with external chiral molecules. These results are in consonance with the electronic absorption titration studies given earlier in the section.

3.3.4. Circular dichorism spectroscopy

The CD spectra have been utilized as a powerful tool for exploring the chiral aspect of compounds and to provide valuable information on the mode of binding between the DNA helix and chiral complexes [17,18,36]. The CD spectra of complexes S-Ni-L, R-Ni-L, S-Cu-L, R-Cu-L, S-Zn-L and R-Zn-L in DMSO are shown in Fig. 6, Figs. S6 and S7.

The CD spectra of free S-Ni-L, S-Cu-L, S-Zn-L and their respective enantiomers R-Ni-L, R-Cu-L, R-Zn-L showed LMCT bands with opposite configuration at ~373 nm. The interaction of complexes with DNA in LMCT region showed decrease in spectral strength by 64%, 59% and 50% for S-Ni-L, S-Cu-L and S-Zn-L while 25%, 30% and 21% for R-Ni-L, R-Cu-L and R-Zn-L respectively. The addition of DNA to the complexes S-Ni-L and R-Ni-L resulted with emergence of a new peak at 305 nm, which showed a red shift of 8 nm and 4 nm respectively on increasing DNA concentration. However,

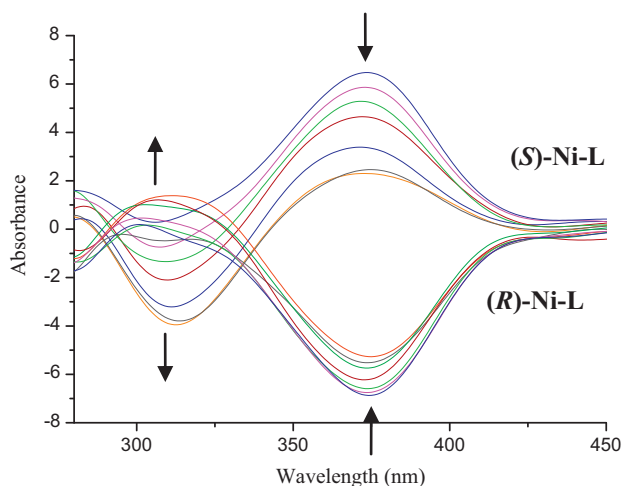


Fig. 6. CD spectra of chiral Schiff base S-Ni-L and R-Ni-L complexes in the presence of increasing concentration of DNA. Complex concentration = 50 μ M.

the complexes S-Cu-L and R-Cu-L showed hypochromism and a blue shift of 7 nm and 5 nm respectively at 328 nm. On the other hand, addition of DNA to the complexes S-Zn-L and R-Zn-L caused hyperchromism and a red shift of 3 nm at 310 nm in both the cases. The above CD spectral changes clearly demonstrate the different matching of enantiomers of the complexes with DNA.

3.3.5. Viscosity study

Viscosity measurement studies on interaction of chiral Schiff base complexes with DNA were carried out to further strengthen the findings on chiral discrimination as obtained in earlier sections. In the absence of crystallographic structural data, hydrodynamic measurement is considered as least ambiguous and the most critical test to find binding mode of DNA with metal complexes. The sensitivity of this method is largely depend on the changes in the length of DNA that occur as result of its different binding modes with guest molecules [18,29].

A classical intercalator such as EB shows a significant increase in the relative viscosity of the DNA solution on intercalation due to the increase in the overall length of DNA and therefore results in an increase in DNA viscosity. In contrast, the groove binding and partial interacting molecules cause minor or no effect on the relative viscosity on DNA [30]. The plots of relative viscosity $(\eta/\eta_0)^{1/3}$ versus [complex]/[DNA] ratio (Fig. 7) illustrated a significant increase in the relative viscosity of DNA in the presence of complexes S-Ni-L and S-Cu-L suggesting their intercalative mode of binding. On the other hand, marginal changes in relative viscosity of DNA with the complexes S-Zn-L, R-Ni-L, R-Cu-L, and R-Zn-L indicates their groove or external binding nature. In a nutshell, binding affinity of the chiral Schiff base complexes with DNA, follows the order of S-Ni-L > S-Cu-L > S-Zn-L > R-Ni-L > R-Cu-L > R-Zn-L.

3.3.6. Thermal denaturation study

The thermal behaviors of DNA in the presence of metal complexes can provide better insight for conformational changes, DNA duplex stability and interaction strength between complexes and DNA. The duplex DNA at its melting temperature unwinds to give single strand DNA and shows an increase in absorbance at 260 nm.

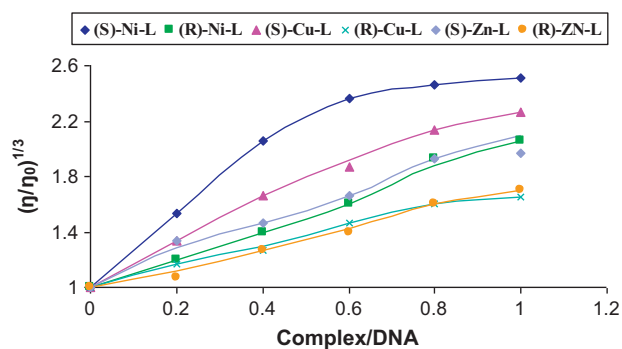


Fig. 7. The relative viscosity of DNA (50 μ M) in the presence of S and R enantiomers of chiral Schiff base metal complexes (0–60 μ M).

Table 3
Stern–Volmer constant of *S* and *R* enantiomers of chiral Schiff base complexes to DNA.

Complexes	λ_{\max} (DNA + EB)	λ_{\max} (DNA + EB + complexes)	$\Delta\lambda$ (nm)	<i>K</i>
<i>S</i> -Ni-L	603	613	10	2.49 ± 0.12
<i>R</i> -Ni-L	603	607	4	1.69 ± 0.13
<i>S</i> -Cu-L	603	626	23	1.18 ± 0.10
<i>R</i> -Cu-L	603	617	14	0.33 ± 0.012
<i>S</i> -Zn-L	612	625	13	0.56 ± 0.010
<i>R</i> -Zn-L	612	621	9	0.37 ± 0.013

A classical intercalator such as EB stabilizes the duplex DNA causing the DNA to melt at higher temperature [37,38]. The melting curves of DNA in the presence and absence of the chiral Schiff base complexes are shown in Fig. 8.

The T_m of DNA was found to be 70 °C, which increased to 80 °C and 75 °C in the presence of *S*-Ni-L and *S*-Cu-L respectively, suggesting their intercalative mode of binding. However, complexes *S*-Zn-L and *R*-Ni-L had little effect on the T_m value of DNA due to poor interaction among them. Ironically, interaction of *R*-Cu-L and *R*-Zn-L with DNA showed a decrease in T_m value (65 °C) for reasons unknown as of now (Fig. 8).

3.3.7. Antioxidant activity

Schiff base metal complexes per se are known to show various biological activities including biocidal and antioxidant activities [39], however chirality aspect of these complexes vis-à-vis bioactivity has not been well explored. In view of this and significant DNA binding affinity shown by the Schiff base complexes used in the present study, it was considered sensible to study other potential aspects of these compounds such as antioxidant and antibacterial activity [40].

Reactive oxygen species (ROS) e.g. superoxide ($O_2^{\bullet-}$) and hydroxyl ($\bullet OH$) radical are responsible for the disintegration of cell membrane and damage to protein and DNA structures. Several non-chiral metal complexes have been reported earlier to show anti-ROS activity [21,25,40–43]. Since the chiral metal complexes studied in the present work showed strong chirality dependent DNA binding, we hypothesized similar manifestation of these complexes on the scavenging of $O_2^{\bullet-}$ and $\bullet OH$ radical activity.

As shown in Fig. 9, increasing concentration (5–25 μM) of all the complexes showed increasing inhibitory activities against ROS. Among the studied complexes *S*-Cu-L and *S*-Zn-L showed highest superoxide scavenging ability of 98% and 99% respectively, in contrast to 64% and 70% inhibition obtained for their *R* counterparts at a concentration of 25 μM . Nickel complexes *S*-Ni-L and *R*-Ni-L also showed considerably high scavenging activity 78% and 56% respectively. As hypothesized, all the *S*-enantiomers of the complexes showed higher $O_2^{\bullet-}$ scavenging activity than their respective *R*-enantiomers.

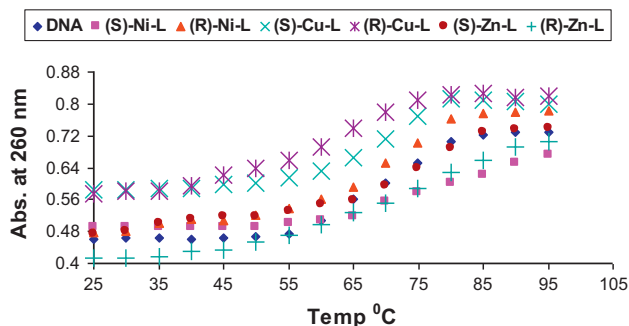


Fig. 8. Thermal denaturation graph of DNA (0.4 mM) in the presence of *S* and *R* enantiomers of chiral Schiff base metal complexes (20 μM).

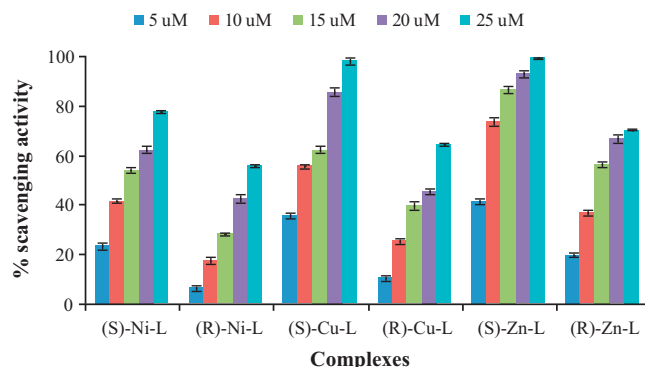


Fig. 9. Scavenging effect of the chiral Schiff base complexes on superoxide radical by MET/VitB₂/NBT system.

The chiral Schiff base metal complexes at the same concentration (5–25 μM) were also screened for the $\bullet OH$ radical scavenging activity (Fig. 10). It is evident from the results that *S*-Cu-L and *S*-Zn-L are better scavenging agents (82% and 89%) than *R*-Cu-L, *R*-Zn-L, *S*-Ni-L and *R*-Ni-L, which showed 51, 54, 73 and 45% scavenging activities respectively at a concentration of 25 μM . Here again, *S*-enantiomers of the complexes were found to be more effective than *R*-enantiomers. It indicates that transition-metal ions like Ni (II), Cu (II) and Zn (II) may have chirality driven differential and selective nature for scavenging $O_2^{\bullet-}$ and $\bullet OH$ radical. This trend can be correlated with the fact that *S* enantiomers of the complexes have shown stronger DNA binding ability than their *R* enantiomers.

3.4. Antibacterial activity

The current issue on drug-resistance pathogens often referred as “super bugs” has led greater demand for the discovery of new chemical scaffolds with antimicrobial activity. Several metal complexes have already shown their worth as antibacterial agents [21,44,45] however, the role of chirality in this aspect is less explored [12]. Therefore, we evaluated the antibacterial activity of the chiral Schiff base complexes using agar cup method with three gram (+), three gram (–) and two fungal pathogens as representative microbes

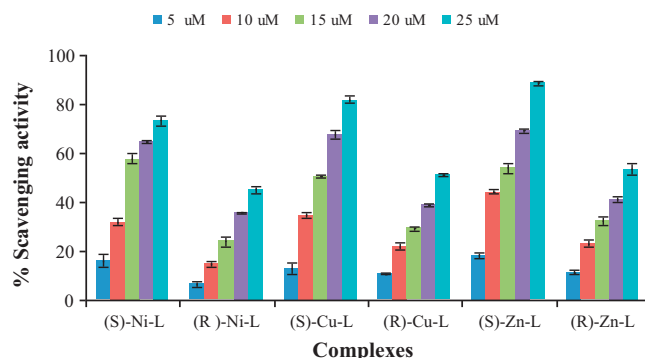


Fig. 10. Scavenging effect of chiral Schiff base metal complexes on hydroxyl radical.

Table 4
Data for antimicrobial activity using chiral Schiff base complexes.

Compound	<i>B. subtilis</i>		<i>B. cereus</i>		<i>S. aureus</i>		<i>E. coli</i>		<i>S. typhi</i>		<i>P. aeruginosa</i>		<i>C. albicans</i>	
	WD ^a	MIC ^b	WD	MIC	WD	MIC	WD	MIC	WD	MIC	WD	MIC	WD	MIC
Control ^d	NA ^c	–	NA	–	NA	–	NA	–	NA	–	NA	–	NA	–
Standard ^e	20	12.5	21	12.5	20	12.5	19	12.5	19	12.5	20	12.5	NA	–
(S)-H ₂ L	NA	–	NA	–	NA	–	NA	–	NA	–	NA	–	NA	–
(R)-H ₂ L	NA	–	NA	–	NA	–	NA	–	NA	–	NA	–	NA	–
(S)-Ni-L	24	12.5	23	12.5	31	12.5	20	12.5	21	12.5	19	12.5	NA	–
(R)-Ni-L	21	25	21	25	29	25	17	25	16	25	16	25	NA	–
(S)-Cu-L	20	12.5	21	12.5	16	12.5	18	12.5	18	12.5	17	12.5	NA	–
(R)-Cu-L	18	25	19	25	18	25	16	25	16	25	15	25	NA	–
(S)-Zn-L	23	12.5	22	12.5	29	12.5	19	12.5	18	12.5	18	12.5	NA	–
(R)-Zn-L	19	25	18	25	25	25	16	25	15	25	16	25	NA	–

^a Diameter of zone of inhibition (mm) including well diameter (6 mm) 200 µg of both compound and antibiotics were used.

^b Minimum inhibitory concentration values given as µg/ml for both compound and antibiotics.

^c Not active.

^d Control DMSO.

^e Standard streptomycin.

(Table 4). It is evident from Table 4 that all the complexes exhibited considerable higher activity against gram (+) and gram (–) bacteria which was as good as the activity found for standard antibiotic—streptomycin. Significantly, the *S* enantiomers of the metal complexes showed higher antibacterial activity than their *R* counterparts. Ironically, none of these complexes showed any activity against fungi. The order of antibacterial activity was found to be *S*-Ni-L > *S*-Zn-L > *R*-Ni-L > *S*-Cu-L > *R*-Zn-L > *R*-Cu-L which also demonstrate the enantiomeric effect.

4. Conclusion

Chiral Schiff base complexes of Ni, Cu and Zn were synthesized in their enantiomerically pure form and were evaluated for their DNA binding ability, antioxidant and antibacterial activity. Various spectrometric methods concluded that the complex *S*-Ni-L has higher DNA binding ability than other chiral Schiff base metal complexes used in the present study. Interestingly, the *S*-Ni-L and *S*-Cu-L complexes bind with DNA through intercalation while *R*-Ni-L, *R*-Cu-L, *S*-Zn-L and *R*-Zn-L interact with DNA through groove or external binding. Discernible differences were observed in the interaction of the different enantiomers with DNA. The *S* enantiomers of the complexes showed stronger DNA binding ability than the *R* enantiomers. Additionally, chiral Schiff base complexes also exhibited excellent antioxidant (O₂^{•–} and •OH radical scavengers) and antibacterial activities. Therefore, the information obtained from the present work would help in developing new potent antioxidants and therapeutic drugs to cure certain valuable diseases.

Acknowledgements

N.H. Khan and N. Pandya are thankful to Council of Scientific & Industrial Research (CSIR) Net Working Project on Catalysis. K. Prathap thankful to CSIR for awarding senior research fellowship.

Appendix A. Supplementary data

Supplementary data associated with this article can be found, in the online version, at doi:10.1016/j.saa.2011.06.002.

References

- [1] K. Tang, H. Gan, Y. Li, L. Chi, T. Sun, H. Fuchs, J. Am. Chem. Soc. 130 (2008) 11284–11285.
- [2] N. Claessens, F. Pierard, C. Bresson, C. Moucheron, A.K.D. Mesmaeker, J. Inorg. Biochem. 101 (2007) 987–996.
- [3] S.K. Teo, W.A. Colburn, W.G. Tracewell, K.A. Kook, D.I. Stirling, M.S. Jaworsky, M.A. Scheffler, S.D. Thomas, O.L. Laskin, Clin. Pharmacokinet. 43 (2004) 311–327.
- [4] B. Lippert, Cisplatin: Chemistry and Biochemistry of a Leading Anticancer Drug, Verlag Helvetica Chimica Acta, Postfach, CH-8042 Zürich, Switzerland, 1999, doi:10.1002/9783906390420.
- [5] M. Chauhan, F. Arjmand, Chem. Biodivers. 3 (2006) 660–676.
- [6] S. Kemp, N.J. Wheate, D.P. Buck, M. Nikac, J.G. Collins, J.R. Aldrich-Wright, J. Inorg. Biochem. 101 (2007) 1049–1058.
- [7] A.P. Noel, J.F. Kane-Maguire, Wheeler, Coord. Chem. Rev. 211 (2001) 145–162.
- [8] S.R. Korupoju, N. Mangayarkarasi, P.S. Zacharias, J. Mizuthani, H. Nishihara, Inorg. Chem. 41 (2002) 4099–4101.
- [9] S. Shi, J. Liu, J. Li, K.C. Zheng, X.M. Huang, C.P. Tan, L.M. Chen, L.N. Ji, J. Inorg. Biochem. 100 (2006) 385–395.
- [10] C.-W. Jiang, J. Inorg. Biochem. 98 (2004) 497–501.
- [11] K. Mudasir, E.T. Wijaya, H. Wahyuni, N. Inoue, Yoshioka, Spectrochim. Acta Part A 66 (2007) 163–170.
- [12] N.H. Khan, N. Pandya, R.I. Kureshy, S.H.R. Abdi, S. Agrawal, H.C. Bajaj, J. Pandya, A. Gupte, Spectrochim. Acta Part A 74 (2009) 113–119.
- [13] F. Westerland, F. Pierard, M.P. Eng, B. Norden, P. Lincoln, J. Phys. Chem. B 109 (2005) 17327–17332.
- [14] P.U. Maheswari, V. Rajendiran, M. Palaniandavar, R. Parthasarathi, V. Subramanian, J. Inorg. Biochem. 100 (2006) 3–17.
- [15] P.U. Maheswari, V. Rajendiran, H. Stoeckli-Evans, M. Palaniandavar, Inorg. Chem. 45 (2006) 37–50.
- [16] N. Mudasir, H. Yoshioka, Inoue, J. Inorg. Biochem. 102 (2008) 1638–1643.
- [17] R. Vijayalakshmi, M. Kanthimathi, R. Parthasarathi, B.U. Nair, Bioorg. Med. Chem. 14 (2006) 3300–3306.
- [18] N.H. Khan, N. Pandya, M. Kumar, P.K. Bera, R.I. Kureshy, S.H.R. Abdi, H.C. Bajaj, Org. Biomol. Chem. 19 (2010) 4297–4307.
- [19] H. Halliwell, Lancet 344 (1994) 721–724.
- [20] D.T. Dexter, J. Sian, S. Rose, Ann. Neurol. 53 (1994) 38–44.
- [21] T. Suksrichavalit, S. Prachayasittikul, C. Nantasenamat, C.I. Na-Ayudhya, V. Prachayasittikul, Eur. J. Med. Chem. 44 (2009) 3259–3265.
- [22] L.Z. Flores-López, M. Parra-Hake, R. Somanathan, P.J. Walsh, Organometallics 19 (2000) 2153–2160.
- [23] A.L. Iglesias, G. Aguirre, R. Somanathan, M. Parra-Hake, Polyhedron 23 (2004) 3051–3062.
- [24] M.C. Prabhakara, B. Basavaraju, H.S. Bhojya Naik, Bioinorg. Chem. Appl. 2007 (2007) 1–7.
- [25] S.R. Doctrow, K. Huffman, C.B. Marcus, G. Tocco, E. Malfroy, C.A. Adinolfi, H. Kruk, K. Baker, N. Lazarowych, J. Mascarenhas, B. Malfroy, J. Med. Chem. 45 (2002) 4549–4558.
- [26] V. Prashanth Kumar, S. Shashidhara, M.M. Kumar, B.Y. Sridhara, Pharm. Biol. 39 (2001) 325–328.
- [27] S.M. Klein, G. Cohen, A.I. Cederbaum, Biochemistry 20 (1981) 6006–6012.
- [28] H. Nash, Biochem. J. 55 (1953) 416–421.
- [29] S. Shi, T.-M. Yao, X.-T. Geng, L.-F. Jiang, J. Liu, Q.-Y. Yang, L.-N. Ji, Chirality 21 (2009) 276–283.
- [30] B. Maity, M. Roy, S. Saha, A.R. Chakravarty, Organometallics 28 (2009) 1495–1505.
- [31] R.B. Nair, E.S. Teng, S.L. Kirkland, C.J. Murphy, Inorg. Chem. 37 (1998) 139–141.
- [32] F. Arjmand, M. Aziz, Eur. J. Med. Chem. 44 (2009) 834–844.
- [33] N. Shahabadi, S. Kashanian, M. Khosravi, M. Mahdavi, Trans. Met. Chem. 35 (2010) 699–705.
- [34] G.-W. Zhang, J.-B. Guo, J.-H. Pan, X.-X. Chen, J.-J. Wang, J. Mol. Struct. 923 (2009) 114–119.
- [35] Z.-C. Liu, B.-D. Wang, Z.-Y. Yang, Y. Li, D.-D. Qin, T.R. Li, Eur. J. Med. Chem. 44 (2009) 4477–4484.

- [36] B. Peng, W.H. Zhou, L. Yan, H.W. Liu, L. Zhu, *Trans. Met. Chem.* 34 (2009) 231–237.
- [37] T.K. Goswami, M. Roy, M. Nethaji, A.R. Chakravarty, *Organometallics* 28 (2009) 1992–1994.
- [38] J.M. Kelly, A.B. Tossi, D.J. McConnell, C. OhUigin, *Nucleic Acids Res.* 13 (1985) 6017–6034.
- [39] S. Kumar, D.N. Dhar, P.N. Saxena, *J. Sci. Ind. Res.* 68 (2009) 181–187.
- [40] Q. Wang, Z.Y. Yang, G.F. Qi, D.D. Qin, *Biometals* 22 (2009) 927–940.
- [41] M. Baudry, S. Etienne, A. Bruce, M. Palucki, E. Jacobsen, B. Malfroy, *Biochem. Biophys. Res. Commun.* 192 (1993) 964–968.
- [42] V. Lanza, G. Vecchio, *J. Inorg. Biochem.* 103 (2009) 381–388.
- [43] A. Colak, U. Terzi, M. Col, S.A. Karaoglu, S. Karaböcek, A. Küçükdumlu, F.A. Ayaz, *Eur. J. Med. Chem.* 45 (2010) 5169–5175.
- [44] S. Shujha, A. Shah, Z.U. Rehman, N. Muhammad, S. Ali, R. Qureshi, N. Khalid, A. Meetsma, *Eur. J. Med. Chem.* 45 (2010) 2902–2911.
- [45] G.B. Bagihalli, P.G. Avaji, S.A. Patil, P.S. Badami, *Eur. J. Med. Chem.* 43 (2008) 2639–2649.